Modeling interfacial flows characterized by large density ratios with the level set method

By M. Raessi AND H. Pitsch

1. Motivation and objectives

Interfacial flows are ubiquitous in industrial and research applications. They are encountered in a variety of important processes including fuel atomization, casting, and oil recovery. Numerical simulations are a powerful and cost-effective tool used to study interfacial flows, but, obviously, accurate simulations are possible only with careful treatment of all important phenomena in such flows. One of the most challenging effects to model in such flows is the large density jump across fluid interfaces. In many industrial applications, the density ratio between fluids is typically about 1000 (e.g., flows of water in air, or molten metals in air). A literature survey suggests that there are several incompressible interfacial flow solvers that, due to numerical stability issues, are limited by some density ratio that is significantly smaller than a realistic value. However, using a realistic density ratio in a problem is essential in order to perform predictive simulations that truly represent the problem of interest.

Rudman (1998) and Bussmann *et al.* (2002) suggest two approaches to modeling flows characterized by high density ratios. Their approaches, however, are only applicable to incompressible flow solvers that employ the volume-of-fluid method (Hirt & Nichols 1981; Scardovelli & Zaleski 1999) for modeling interface kinematics. But, in an equally common group of incompressible flow solvers, the level set method (Osher & Sethian 1988; Osher & Fedkiw 2001; Sethian 2001) is used to model the evolution of fluid interfaces. Following the ideas presented by Rudman (1998) and Bussmann *et al.* (2002), we proposed a level set-based method to model interfacial flows with high density ratios (Raessi 2008). In this method, mass and momentum are transported consistently by using the same flux densities. Furthermore, the interface location (i.e., density discontinuity) is taken into account in the calculation of flux densities. The input of this method is a signed distance function to the interface, and therefore, this method can be easily employed by any level set-based flow solver, regardless of the method used to solve for the evolution of the level set function. Raessi (2008) focused on the numerical algorithm itself; here, after a brief review of the method, we assess the performance of the algorithm in a flow solver and use a variety of test cases in which the density ratio ranges between 650 and 1000.

2. Governing equations

The governing equations for an interfacial flow of Newtonian, immiscible fluids are conservation of mass and momentum:

$$\frac{\partial \rho}{\partial t} + \nabla \cdot (\rho \boldsymbol{U}) = 0, \tag{2.1}$$

$$\frac{\partial (\rho \boldsymbol{U})}{\partial t} + \nabla \cdot (\rho \boldsymbol{U}\boldsymbol{U}) = -\nabla p + \nabla \cdot \tau + \boldsymbol{F}_B, \tag{2.2}$$

where $\boldsymbol{U}$ denotes velocity, p pressure, τ the shear stress tensor $\tau = \mu(\nabla \boldsymbol{U} + \nabla \boldsymbol{U}^T)$, and $\boldsymbol{F}_B$ any body forces.

The following conditions apply across fluid interface: For viscous fluids with no mass interchange between two different phases of a single substance, the velocity components normal and tangential to fluid interfaces are equal in both fluids (Bird *et al.* 2002). That is,

$$[\boldsymbol{U}] \equiv \boldsymbol{U}^{(1)} - \boldsymbol{U}^{(2)} = 0, \tag{2.3}$$

where superscripts (1) and (2) denote fluids 1 and 2.

Furthermore, the following jump condition for the stress tensor exists across fluid interfaces (Landau & Lifshitz 1987):

$$[(-pI + \tau) \cdot \hat{n}] = \sigma \kappa \hat{n}, \tag{2.4}$$

where $\hat{n}$ is the unit normal vector to the interface, σ is the surface tension coefficient (assumed constant), and κ is interface curvature.

Using the level set method to model the interface kinematics, we solve the following transport equation for a scalar indicator function $G = G(\boldsymbol{x}, t)$:

$$\frac{\partial G}{\partial t} + \boldsymbol{U} \cdot \nabla G = 0. \tag{2.5}$$

Although G can be any smooth function, the most commonly used one is a signed distance function. The interface is represented by an isosurface $G_0 = 0$. We solve a single set of Eqs. (2.1) and (2.2) in all fluids; the fluid properties (assumed constant in each fluid) are determined from G at any point.

3. Numerical method

Before presenting the details of the numerical method, it is worth noting that a common approach to modeling incompressible interfacial flows is to solve Eq. (2.2) in the following non-conservative form:

$$\frac{\partial \boldsymbol{U}}{\partial t} + \boldsymbol{U} \cdot \nabla \boldsymbol{U} = \frac{1}{\rho} \left(-\nabla p + \nabla \cdot \tau + \boldsymbol{F}_B \right). \tag{3.1}$$

As discussed by Bussmann *et al.* (2002), the above non-conservative formulation is likely fine at low density ratios where the jump in fluid densities has less importance in the change of momentum in interface cells than local variations of velocity. However, as shown in section 4, in flows with high density ratios (~ 1000), solving the non-conservative form in the momentum transport step results in large errors. Therefore, in our new method, as the first step in the time advancement, the following equation is solved to transport momentum:

$$\frac{\partial \rho \boldsymbol{U}}{\partial t} = -\nabla \cdot (\rho \boldsymbol{U} \boldsymbol{U}). \tag{3.2}$$

That is, at the momentum transport step, we evaluate an interim velocity $\boldsymbol{U}^*$ via†,

$$\frac{\rho^{n+1} \boldsymbol{U}^* - (\rho \boldsymbol{U})^n}{\Delta t} = -\nabla \cdot (\rho \boldsymbol{U} \boldsymbol{U})^n. \tag{3.3}$$

The new method was implemented in the framework of NGA, which is an in-house

† First-order time discretization is for demonstration only; in practice the temporal discretization is second-order accurate or higher.

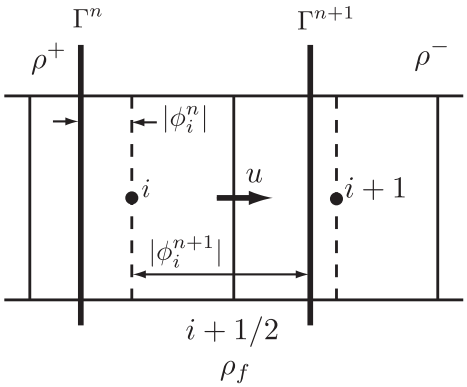

FIGURE 1. Calculation of flux density across surface i from the signed distance function ϕ at two consecutive time levels n and $n+1$.

code described extensively in Desjardins *et al.* (2008*a*,*b*) and Desjardins & Pitsch (2009). NGA is a structured, finite-difference flow solver with staggered arrangement of variables. It is a parallel code designed for direct numerical simulation and large-eddy simulation of turbulent reactive flows.

Following the momentum transport step, we obtain $\boldsymbol{U}$ from $\rho\boldsymbol{U}$ and return to the non-conservative formulation. We then follow the methods described in (Desjardins *et al.* 2008*b*) to implement the remaining terms in Eq. 3.1. These methods include the Ghost-Fluid method (GFM) (Desjardins *et al.* 2008*b*; Kang *et al.* 2000), which is employed to account for density jumps in the pressure term as well as to implement the surface tension force.

To solve Eq. 3.2 for momentum transport, we require density in the momentum flux term. Employing the method described in (Raessi 2008), we calculate flux densities by using a signed distance function at two consecutive time levels and taking into account the discontinuity of the density field. For instance, consider the case shown in Fig. 1, where Γ denotes the interface between fluids with density ρ^+ and ρ^-. Γ moves with velocity u during time levels n and $n+1$. Using the method described in (Raessi 2008), the flux density across surface i (dashed line in Fig. 1), which is denoted by $\hat{\rho}_i$, is

$$\hat{\rho}_i = \frac{|\phi_i^n|\rho^- + |\phi_i^{n+1}|\rho^+}{|\phi_i^n| + |\phi_i^{n+1}|}, \tag{3.4}$$

where ϕ_i^n and ϕ_i^{n+1} are the signed distance functions at point i. Across surface $i+1$, we have $\hat{\rho}_{i+1} = \rho^-$.

To obtain $\boldsymbol{U}$ from $\rho\boldsymbol{U}$, densities at cell faces (where $\boldsymbol{U}$ is defined) are required; we denote density on cell faces by ρ_f. To calculate ρ_f^{n+1}, we solve the following conservation of mass equation

$$\frac{\partial \rho_f}{\partial t} = -\nabla \cdot (\rho \mathbf{U}), \tag{3.5}$$

where the initial condition is computed based on the level set field at time n. The crucial point in solving Eq. 3.5 is to use the same flux densities as those used in Eq. 3.2. This ensures consistent mass and momentum transports. For the example shown in Fig. 1, ρ_f

on face $i+1/2$ can be calculated from Eq. 3.5 as follows: †

$$\frac{\rho_f^{n+1}-\rho_f^n}{\Delta t}=-\frac{u}{\Delta x}(\rho^- -\hat{\rho})=-\frac{u}{\Delta x}\frac{|\phi_i^{n+1}|(\rho^- -\rho^+)}{|\phi_i^n|+|\phi_i^{n+1}|}, \tag{3.6}$$

where Δx denotes the distance between points i and $i+1$ and Δt is the time step between times n and $n+1$. Because $u\Delta t=|\phi_i^n|+|\phi_i^{n+1}|$,

$$\rho_f^{n+1}-\rho_f^n=\frac{|\phi_i^{n+1}|}{\Delta x}(\rho^+-\rho^-) \tag{3.7}$$

And, because $\rho_f^n=\rho^-$, we obtain

$$\rho_f^{n+1}=\frac{|\phi_i^{n+1}|\rho^+ +(\Delta x-|\phi_i^{n+1}|)\rho^-}{\Delta x}, \tag{3.8}$$

which is a convex combination of ρ^+ and ρ^-.

An alternative to the above approach is to use the level set function at time $n+1$ to calculate ρ_f^{n+1} but that does not guarantee consistent mass and momentum transport simply because the advections of momentum and the level set function are not coupled. Small discrepancies between the transport of momentum and the level set function cause mismatch between mass and momentum and result in non-physical velocities, especially evident at large density ratios.

For calculation of flux density in higher dimension, see Raessi (2008).

4. Results

This section presents several test cases for the new method (in which Eq. 3.2 is solved for momentum transport) as well as comparisons between the results of the new method and the non-conservative formulation (Eq. 3.1). Note that the only difference between the two formulations lies in the momentum transport (treatment of the convective term); the other terms are treated exactly the same. To assess the performance of the new method, we begin with test cases in which the geometry of fluid interfaces is relatively smooth and then consider problems that involve complex interface geometries. In these test cases, the density ratio is high and ranges from 650 to 1000.

4.1. *Collapse of a water column*

We first begin with a test case that was originally presented in Raessi (2008), where only qualitative comparisons between the simulations and experimental results were given. Here, we present a quantitative comparison. For the sake of completeness, we first review the test case: consider a two-dimensional water (fluid 1) column in air (fluid 2), shown in Fig. 2, which corresponds to the experimental results of Martin & Moyce (1952). The initial height and width of the column are both 5.715 cm. Here $\rho_1=1000\,\mathrm{kg/m^3}$, $\rho_2=1.226\,\mathrm{kg/m^3}$, $\mu_1=1.137\times10^{-3}\,\mathrm{kg/ms}$, $\mu_2=1.78\times10^{-5}\,\mathrm{kg/ms}$, $\sigma=0.0728\,\mathrm{N/m}$, $g=9.81\,\mathrm{m/s^2}$. Taking the initial column width, a, as the characteristic length, we have $\mathrm{Fr}=u/\sqrt{ag}=1$, $\mathrm{We}=\rho u^2a/\sigma=440$, $\mathrm{Re}=\rho ua/\mu=37635$. The domain size is 40×10 cm, and is discretized by 256×64 uniform grid points.

The results obtained from the new method and the non-conservative formulation are illustrated in Fig. 2(a) and (b), respectively. The non-dimensional spread rates for these

† First-order time discretization is for demonstration only; in practice the temporal discretization is second-order accurate or higher.

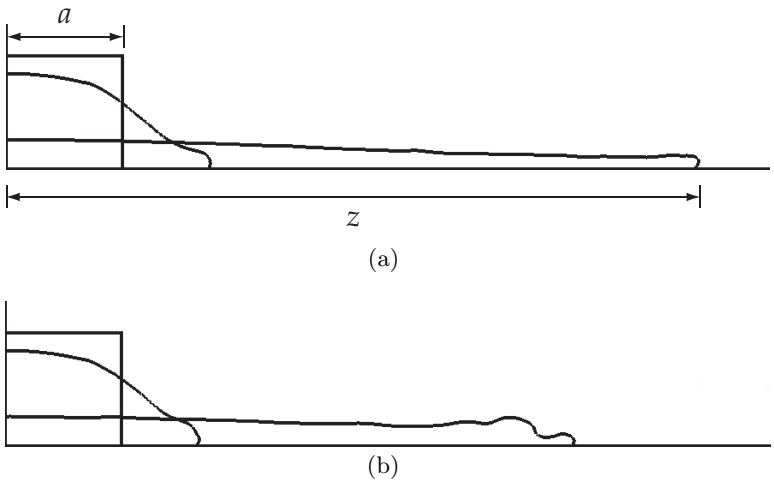

FIGURE 2. Collapse and spread of a water column in air simulated by (a) the new method and (b) the non-conservative formulation of the flow equation (density ratio: 815).

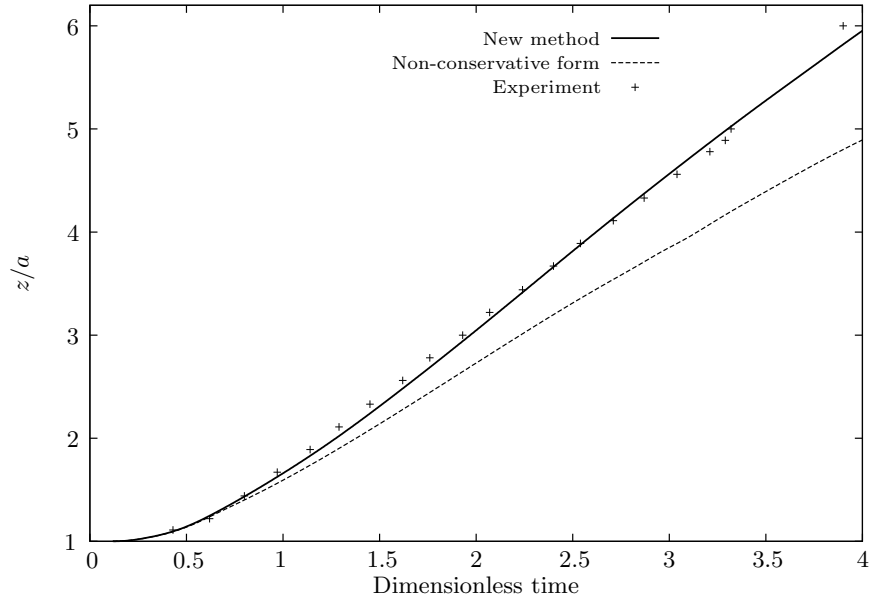

FIGURE 3. Non-dimensional front position of collapsing water columns in air, shown in Fig. 2, versus dimensionless time (density ratio: 815).

results are shown in Fig. 3 for each formulation, and are compared with the experimental results (Martin & Moyce 1952). As seen, the results of the non-conservative form shows slow spread rate, which is also evident in Fig. 2(b). This is due to errors in momentum transfer across the interface, which do not vanish by increasing the grid resolution. These errors manifest themselves as slowdown of the denser fluid (water) by the lighter fluid (air), which is obviously non-physical. The results of the new method do not show

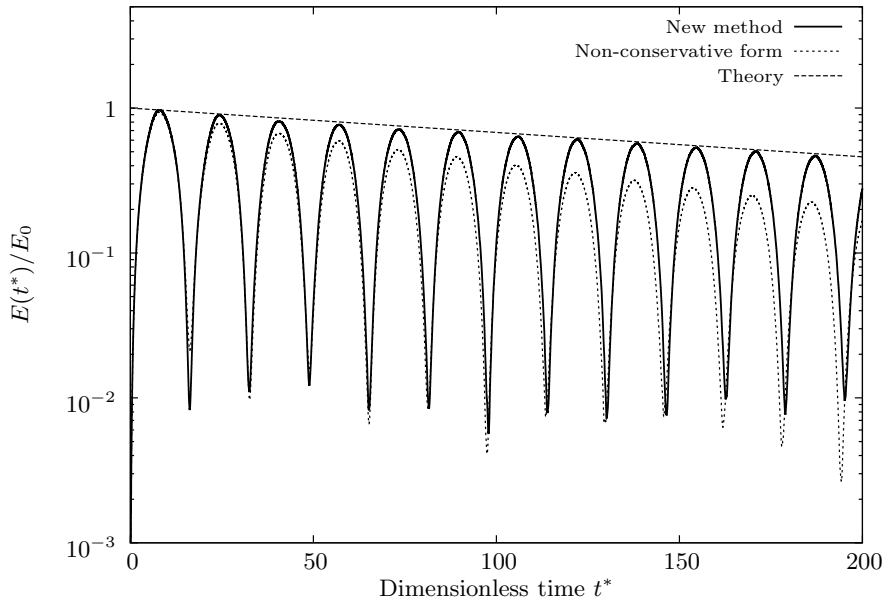

FIGURE 4. Decay of the total energy of an oscillating viscous drop (density ratio: 1000).

this non-physical behavior. The spread rate predicted by the new method matches the experimental spread rate very well.

4.2. *Oscillations of a viscous drop*

As another validation test case, we study the oscillation of a viscous drop owing to surface tension effect. The initial geometry is an ellipse of fluid 1, with semimajor axes of 0.3 and 0.2 in the x and y-directions, respectively, positioned at the center of a 1×1 domain, otherwise filled with fluid 2. Here $\rho_1 = 1000\,\mathrm{kg/m^3}$, $\rho_2 = 1\,\mathrm{kg/m^3}$, $\mu_1 = \mu_2 = 7.5 \times 10^{-3}\,\mathrm{kg/ms}$, and $\sigma = 0.1\,\mathrm{N/m}$.

From the theoretical work of Rush & Nadim (2000), the decay of the total energy of the drop, denoted by E, is given by

$$E(t^*) = E_0 e^{-2n(n-1)\nu^* t^*}, \tag{4.1}$$

where t^* is the dimensionless time, n is the mode number, $\nu^* = \mu_1/\sqrt{\rho_1 \sigma L}$ is a dimensionless parameter (Ohnesorge number), and L is the drop dimension.

We ran the simulation to $t^* = 200$ using both the new method and the non-conservative formulation. Fig. 4 shows the decay of the total energy in time. The new method predicts the theoretical decay rate very well. However, in the results obtained with the non-conservative formulation, the decay rate is incorrectly faster owing to numerical errors in momentum transport. Similar to the previous test case, in the results obtained from the non-conservative formulation, the heavier fluid seems to be incorrectly slowed down by the lighter fluid owing to the above errors, which, again, do not vanish with grid refinement.

4.3. *A bursting bubble*

We adopted the next test case from (Rudman 1998). Consider a two-dimensional bubble of fluid 1, of diameter $D = 1$ (all parameters in this test case are dimensionless), posi-

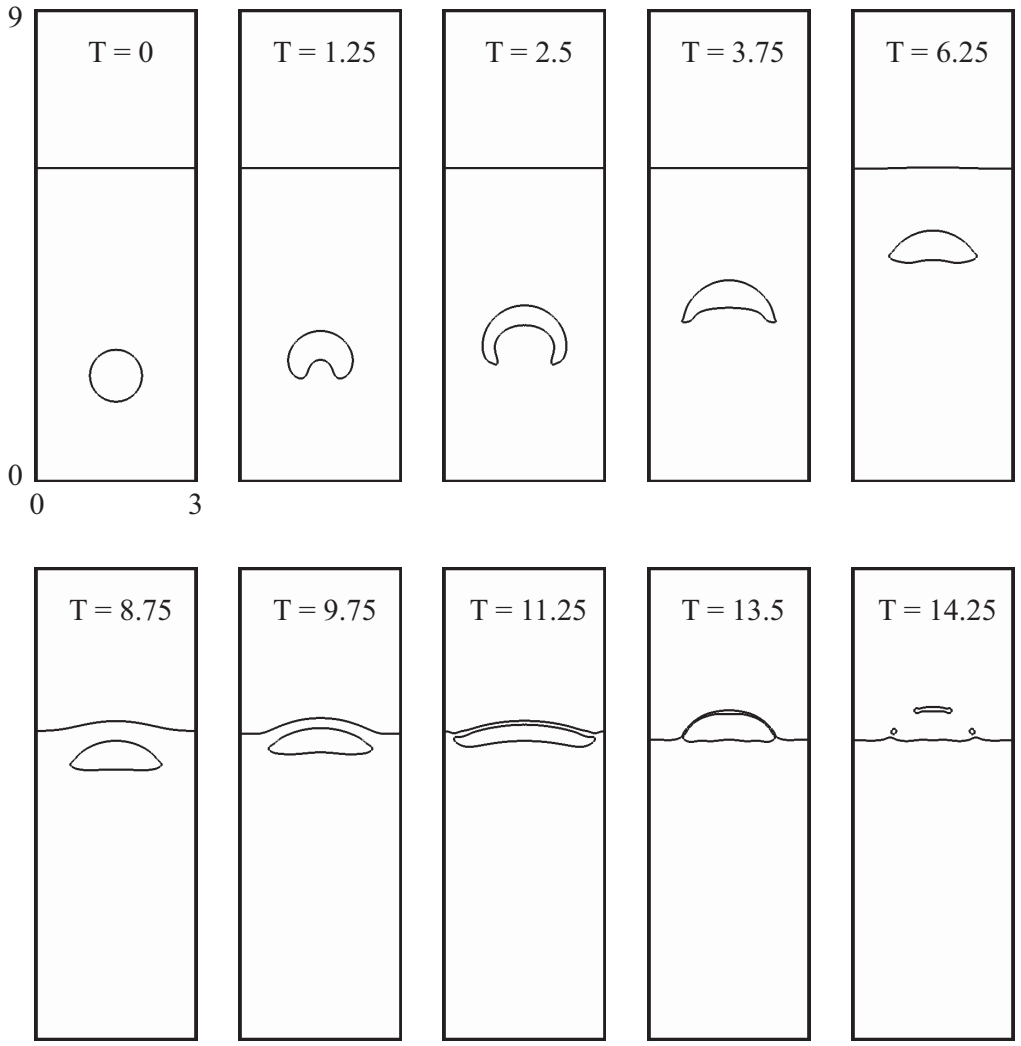

FIGURE 5. Rise, deformation, and burst of a two-dimensional bubble in a liquid pool (density ratio: 1000).

tioned at (1.5,2) in a 3×9 container filled with fluid 2 up to height $h = 6$ (see Fig. 5). Similar to (Rudman 1998), we choose $\rho_1 = 1000$, $\rho_2 = 1$, Fr = 1, We = 25, and Re = 500.

Fig. 5 illustrates the results of the new formulation at 192×576 grid resolution, at various non-dimensional times $\mathrm{T} = t\sqrt{g/D}$. At the early stages of its rise ($\mathrm{T} \leq 3.75$), the bubble deforms to a crescent, but then forms a cap-shape ($6.25 \leq \mathrm{T} \leq 8.75$). During $6.25 \leq \mathrm{T} \leq 8.75$, apart from very small oscillations on its trailing edge, the bubble has a steady shape. The free surface also starts to rise during this period. As the bubble approaches the free surface, it is deformed and flattened by surface tension forces along the free surface ($9.75 \leq \mathrm{T} \leq 11.25$). The bubble again deforms to a cap-shape, and a thin layer of liquid is formed above the bubble ($\mathrm{T} = 13.5$). The layer then thins and ruptures through capillary instability and forms small drops, which fall to the pool.

These results agree very well with those presented by Rudman (1998), especially during

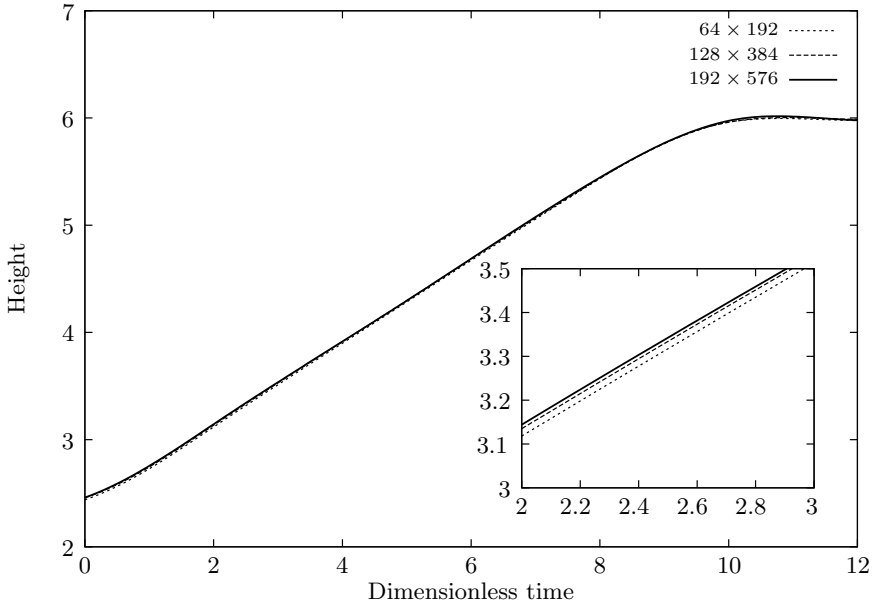

FIGURE 6. Bubble height versus dimensionless time for different mesh resolutions.

bubble rise. The only difference lies in the timing and dynamics of the bubble burst. These differences are likely the result of the approaches used to model interface kinematics employed in each work. We use a spectrally refined interface (SRI) approach (Desjardins & Pitsch 2009), which provides a subgrid representation of fluid interfaces. Although Rudman (1998) used the volume-of-fluid (VOF) method on a grid twice as fine as the flow solver grid, the VOF method does not allow a subgrid representation of the interface. Therefore, unlike the VOF method, thin fluid ligaments can be represented by the SRI approach, which can result in a different rupture dynamics.

Next, we present the position (height) of the bubble's top-most point versus T in Fig. 6, for different grid resolutions. Similar to Rudman (1998), the results obtained with different resolutions are very close to each other, which indicates that the flow is well resolved even at the coarse resolution. The average rise velocity predicted by the simulations in this work is 0.38, which agrees well with that obtained in Rudman (1998).

4.4. *Liquid sheet breakup*

We conclude with a test case that involves more complicated interface topologies. This test is based on the experimental work of Stapper *et al.* (1992). Consider a two-dimensional liquid ethanol (fluid 1) sheet of thickness $d = 508\,\mu$m, injected at $U_1 = 5\,$m/s with shear air (fluid 2) flowing on its top and bottom surfaces at 30 m/s. Here $\rho_1 = 789\,\mathrm{kg/m^3}$, $\rho_2 = 1.226\,\mathrm{kg/m^3}$, $\mu_1 = 1.39 \times 10^{-3}\,\mathrm{kg/ms}$, $\mu_2 = 1.78 \times 10^{-5}\,\mathrm{kg/ms}$, and $\sigma = 0.022\,\mathrm{N/m}$ (ethanol properties are taken from (Stapper *et al.* 1992)). Taking the relative velocity as the characteristic velocity and d as the characteristic length, the dimensionless numbers based on ethanol properties are $\mathrm{Oh} = \mu/\sqrt{\rho\sigma d} = 0.015$, $\mathrm{We} = 11400$, and $\mathrm{Re} = 7200$.

We used a $5 \times 1\,$cm computational domain discretized by 2560×512 uniformly distributed grid points. The lip of the nozzle is included in the computational domain too, and is $500\,\mu$m long and $150\,\mu$m thick on each side.

Fig. 7 illustrates the results at non-dimensional times $\mathrm{T} = td/U_1$. The liquid interface

FIGURE 7. Breakup of ethanol in shear air flow (density ratio: 650).

experiences complex deformations: shortly after liquid injection, instabilities start to appear and grow along the interface (T = 50). We also observe liquid ligaments extending from the surface of the liquid sheet. The ligaments either collapse on the liquid surface and trap air in some cases, or detach from the liquid sheet and break up into smaller structures and droplets. We also observe that at some locations the liquid sheet breaks because of necking and forms isolated liquid structures. These structures further break up into smaller liquid structures and drops (T = 70 to 82.5). Note that the main focus in this simulation was on assessing the performance of the new formulation in complex interface deformations during the primary breakup of the liquid sheet, and not on resolving small liquid structures detaching from the liquid sheet, which eventually disappear as their sizes fall below the grid size. Finally, the liquid sheet develops oscillations near the injector. This behavior, which was also observed in the experiments by Stapper *et al.* (1992), is likely because of pressure oscillations caused by liquid-air interaction.

5. Conclusion

A new level set based method for modeling incompressible, interfacial flows characterized by large density ratios was presented. In this method, the conservative form of the flow equation is solved to transport momentum. Using the signed distance function at two consecutive time levels, density of mass and momentum fluxes are calculated by taking into account the discontinuity in the density field. Then, using the same flux densities, mass and momentum are transported consistently. The new formulation was used to simulate various test cases, in which the density ratio ranges from 650 to 1000. The results clearly demonstrate the efficacy of the new method, as they agree very well with the experimental/theoretical results. Furthermore, the new method is well capable of handling cases where fluid interfaces undergo large deformations (e.g., breakup of a liquid sheet).

6. Future work

Future work will focus on extending the new method for three-dimensional flows. Furthermore, by exploiting the important capability of the new method to handle interfacial flows with large density ratios, it is now possible to run simulations of primary breakup of liquids using realistic density ratios. These simulations will clearly determine the effects of density ratio on the primary breakup and resulting liquid structures.

Acknowledgments

The insightful comments of Dr. E. Johnsen are greatly appreciated. Financial support by NASA is gratefully acknowledged.

REFERENCES

Bird, R. B., Stewart, W. E. & Lightfoot, E. N. 2002 *Transport Phenomena*, 2nd edn. New York: John Wiley and Sons.

Bussmann, M., Kothe, D. B. & Sicilian, J. M. 2002 Modeling high density ratio incompressible interfacial flows. In *Proceedings of ASME 2002 Fluids Engineering Division Summer Meeting*. Montreal, Canada.

Desjardins, O., Blanquart, G., Balarac, G. & Pitsch, H. 2008*a* High order conservative finite difference scheme for variable density low Mach number turbulent flows. *J. Comput. Phys.* **227** (15), 7125–7159.

Desjardins, O., Moureau, V. & Pitsch, H. 2008*b* An accurate conservative level set/ghost fluid method for simulating turbulent atomization. *J. Comput. Phys.* **227** (18), 8395–8416.

Desjardins, O. & Pitsch, H. 2009 A spectrally refined interface approach for simulating multiphase flows. *J. Comput. Phys.* **228** (5), 1658–1677.

Hirt, C. W. & Nichols, B. D. 1981 Volume of fluid (VOF) method for the dynamics of free boundaries. *J. Comput. Phys.* **39**, 201–225.

Kang, M., Fedkiw, R. & Liu, X.-D. 2000 A boundary condition capturing method for multiphase incompressible flow. *J. Sci. Comput.* **15** (3), 323–360.

Landau, L. D. & Lifshitz, E. M. 1987 *Fluid Mechanics*, 2nd edn. Oxford: Pergamon Press.

Martin, J. & Moyce, W. 1952 An experimental study of the collapse of liquid columns on a rigid horizontal plane. *Philos. Trans. R. Soc. London, Ser. A* **244**, 312–324.

Osher, S. & Fedkiw, R. 2001 Level set methods: an overview and some recent results. *J. Comput. Phys.* **169**, 463–502.

Osher, S. & Sethian, J. A. 1988 Fronts propagating with curvature-dependent speed: Algorithms based on Hamilton-Jacobi formulations. *J. Comput. Phys.* **79**, 12–49.

Raessi, M. 2008 A level set based method for calculating flux densities in two-phase flows. In *Annual Research Briefs-2008*, pp. 467–478. Center for Turbulence Research, Stanford, CA.

Rudman, M. 1998 A volume-tracking method for incompressible multifluid flows with large density variations. *Int. J. Numer. Meth. Fluids* **28**, 357–378.

Rush, B. M. & Nadim, A. 2000 The shape oscillations of a two-dimensional drop including viscous effects. *Eng. Anal. Boundary Elem.* **24**, 43–51.

Scardovelli, R. & Zaleski, S. 1999 Direct numerical simulation of free-surface and interfacial flow. *Annu. Rev. Fluid Mech.* **31**, 567–603.

Sethian, J. A. 2001 Evolution, implementation, and application of level set and fast marching methods for advancing fronts. *J. Comput. Phys.* **169** (2), 503–555.

Stapper, B., Sowa, W. & Samuelsen, G. 1992 An experimental study of the effects of liquid properties on the breakup of a two-dimensional liquid sheet. *J. Eng. Gas Turbines Power* **114**, 39–45.